Article

"Doing More with Less": Ni(II)@ORMOSIL, a Novel Sol-Gel Pre-Catalyst for the Reduction of Nitrobenzene

Michael Meistelman [1], Dan Meyerstein [2,3,*], Ariela Burg [4], Dror Shamir [5] and Yael Albo [1,*]

1   Department of Chemical Engineering, Centre for Radical Reactions, Ariel University, Ariel 4070000, Israel; michaelme@ariel.ac.il
2   Department of Chemical Sciences, Centre for Radical Reactions, Ariel 4070000, Israel
3   Chemistry Department, Ben-Gurion University, Beer-Sheva 8410501, Israel
4   Department of Chemical Engineering, Sami Shamoon College of Engineering, Beer-Sheva 8410802, Israel; arielab@sce.ac.il
5   Department of Chemistry, Nuclear Research Centre Negev, Beer-Sheva 8419001, Israel; drorshamir@gmail.com
*   Correspondence: danm@ariel.ac.il (D.M.); yaelyt@ariel.ac.il (Y.A.)

Abstract: Reduction of nitrobenzene with $NaBH_4$ using zero-valent iron nanoparticles (ZVI-NPs) and $NiCl_2 \cdot 6H_2O$ incorporated in organically modified hybrid silica matrices as ZVI@ORMOSIL and Ni(II)@ORMOSIL catalysts is proposed as a remediation strategy. Ni(II)@ORMOSIL is prepared by ion-exchanging H^+ of the ORMOSIL matrix with Ni^{II}. Ni(II)@ORMOSIL is a pre-catalyst that undergoes reduction by $NaBH_4$ by an in-situ reaction and promotes nitrobenzene reduction by the unconsumed $NaBH_4$, leading to sparing use of the catalyst. Ni(II)@ORMOSIL undergoes color change from green to black in this process, returning to a green hue after washing and drying. Nitrobenzene reductions were examined in aqueous acetonitrile solvent mixtures, and the reduction cascade produced the reaction end-products with catalytic implications. Plausible mechanisms of ZVI@ORMOSIL and Ni(II)@ORMOSIL catalyzed reductions of nitrobenzene are discussed. This work is the first to report M(II)@ORMOSIL pre-catalysts for in-situ reduction of nitrobenzene, and expands the scope of the ORMOSIL series of catalysts for the reduction of polluting compounds. This approach enables the development of catalysts that use very low concentrations of transition metal cations.

Keywords: nickel; nitrobenzene; catalysis; reduction; sol-gel

1. Introduction

Nitrobenzene, NB, is an abundant environmental pollutant. It is used in the synthesis of explosives, organophosphate pesticides, herbicides [1], dyes, fungicides [2], lubricating motor oils, solvents, polishes [3,4], drugs, and synthetic rubber [3]. NB is carcinogenic via all routes of exposure (skin, oral, inhalation) [3,5,6]. This USEPA "priority pollutant" is known to accumulate in groundwaters [7,8]. Nitrobenzene is a representative of the nitroarene group. It is used as a probe compound to study the catalytic reduction of nitroarenes. In these reductions, the nitrogen atom oxidation state (III) is reduced to (-III); i.e., this is a 6-electron reduction process [1].

In principle, NB can be decomposed via advanced oxidation technologies, like other aromatic pollutants, but this will result in the release of NO_2 or HNO_3, which is clearly undesired. Therefore, the degradation of NB and other nitroarenes is performed via reduction of the nitro group [9]. Adding an iron powder to anaerobic sludge accelerates NB reduction [9]. However, Zero Valent Iron (ZVI) is easily aggregated [10] and forms a passivation layer of oxide/hydroxides [10,11]; this limits its application. Recently it was shown that ZVI nanoparticles encapsulated in organically modified silica (ORMOSIL) matrices prepared via the sol-gel synthesis route are proficient catalysts in the reduction of

halo-acetic acids, nitrophenol [12] and chloroacetamides pollutants with $NaBH_4$ [13]. ZVI with $NaBH_4$ (SBH) efficiently reduces nitrophenol to aminophenol [14]. The activation of ZVI by etching the oxide layer results in smaller particles [14], thus increasing its active surface and facilitating the catalytic reduction process [14].

It was shown that the reduction of transition metal complexes, M = Fe^{II}; Co^{II}; Ni^{II}; Cu^{II}, by BH_4^- in the presence of nitro-aromatic pollutants leads to their catalytic reduction in aqueous and alcoholic media [15,16]. These results suggest that M^0-NPs formed in situ act as catalysts in the reduction process. As such "homogeneous" catalysts cannot be recycled, efforts to develop analogous heterogeneous catalysts were conducted. For nickel, they have included using nickel-nanowires [17], nickel ion-exchanged zeolites [18] and Ni^0, Ni^0-Al_2O_3 and Ni^0-Ca^{II}-Al_2O_3 in xerogel matrices [19]. Recently it was shown that nickel ions can be easily ion-exchanged into ORMOSIL matrices [20]. These matrices containing nickel ions were shown to be good catalysts for water oxidation in the presence of bicarbonate [20].

It seemed of interest to examine whether such nickel ion-exchanged ORMOSIL matrices also act as pre-catalysts for the reduction of nitro-aromatic compounds. If indeed so, this is of interest as these matrices are easy to prepare, stable, and can be easily recycled. Furthermore, one can control the concentration of nickel ions in the matrix. Here it is not clear that more nickel ions will form a better catalyst as lower concentrations of Ni(II) cations, homogeneously distributed in the matrix, are expected to form smaller Ni^0-NPs upon reduction. The smaller NPs are expected to be better catalysts. Another advantage of such ORMOSIL catalytic matrices is that they enable to perform the reactions in different solvents. Though, clearly, if BH_4^- is used, some water, or an ROH solvent, will have to be used, as $B(OH)_4^-$ or $B(OR)_4^-$ are among the final products.

In this study, it was decided to check whether Ni(II)-ORMOSIL matrices are efficient pre-catalysts for the reduction of nitrobenzene. The catalytic efficiency of the Ni(II)@ORMOSIL matrices is compared to Fe^0-ORMOSIL matrices. The effect of the nature of the solvent used was checked by using different volumetric ratios of H_2O and CH_3CN. The effect of the concentration of Ni^{2+} in the matrix was analyzed. The results clearly demonstrate that Ni(II)@ORMOSIL matrices are efficient, recyclable catalysts for nitro-arene reductions.

2. Results and Discussion

2.1. Catalyst Characterization

2.1.1. ZVI@ORMOSIL Characterization

ZVI@ORMOSIL characterization was described previously [13]; synthetic procedures were not changed. Interconnected bottleneck constrictions were attributed to the mesoporous structure, possibly contributing to the diffusion-controlled reduction reaction rates. 1.0% ZVI@ORMOSIL exhibited a surface area of 751 (m^2/g) with 4.7 nm pore diameter (nm) and 0.73 (cm^3/g) pore volume. 0.2% atomic composition of ZVI was observed with the XPS surface composition analysis. The obtained catalyst powder has magnetic properties. Additionally, the presence of ZVI in the bulk of the ZVI@ORMOSIL matrix was recently verified by XRF analysis. X-ray fluorescence is a valuable method for detecting the elemental metal composition in ORMOSIL gels [21]. Identification is achieved by comparing typical Kα1 and Kβ1 for each metal as fingerprint identification. The X-Ray fluorescence emission spectrum that was measured for 1% mol ZVI@ORMOSIL exhibits typical Kα1 at 6.4 KeV and Kβ1 at 7.06 Kev, indicating the presence of iron in the bulk of the material, Figure 1.

2.1.2. Ni(II)@ORMOSIL Characterization

Ni(II)@ORMOSIL raw gel (Figure S1), obtained according to the procedure described in Section 3.2.2, has a "green hue" [22] typical of divalent nickel with an octahedral coordination sphere. Metal presence in Vycor and silica gel composition can be verified by their spectroscopic properties [23,24]. The UV-Vis absorption spectrum of the Ni(II) is stable [25] and does not change in silica gel [26]. The UV-Vis spectrum of 0.14 M $NiCl_2·6H_2O$ solution

and 10% Ni(II)@ORMOSIL show similar absorption peaks at about 400 nm (Figure S2). Surface morphology of 1% Ni(II)ORMOSIL was examined by STEM/EDAX analysis, and the elemental composition was probed at three different regions of the catalyst (Figure 2).
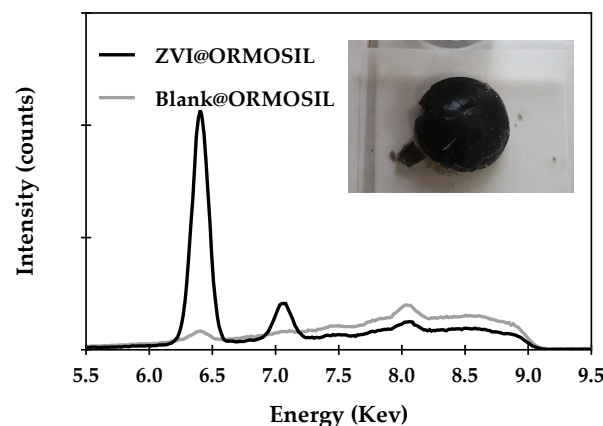

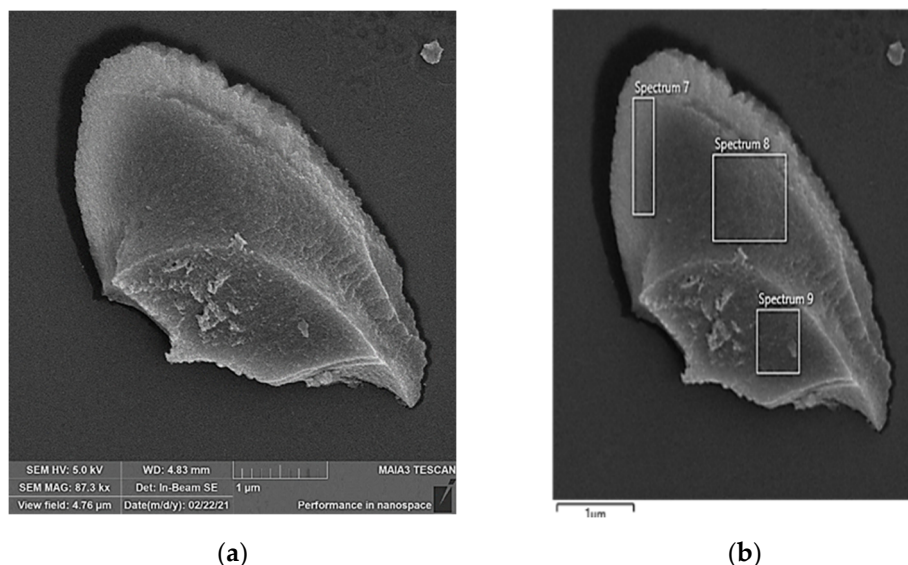**Figure 1.** XRF spectra; Blank@ORMOSIL-grey, ZVI@ORMOSIL-black, Inset: black ZVI@ORMOSIL.

(**a**)　　　　　　　　　　　　　　　　(**b**)

Figure 2. Scanning electron microscope images; 1.0% Ni (II)@ORMOSIL catalyst matrix (**a**,**b**), an image in which the three regions probed by EDS analysis are marked (**b**).

The drying stage of this amorphous silica monolith produces its final morphology through densification and a non-uniform matrix shrinkage [13]. The recorded elemental spectra reveal little Ni presence at the surface, Figure 3. Different amounts of detected nickel traces with high variability (spectrum 7, spectrum 8, and 9) strengthen the need for a more surface-sensitive approach. The EDAX and XPS elemental composition detection methods have different probing depths. The combination of both techniques ensures the detection of the catalyst species in the bulk of the composite material, at the surface layers, or both [27]. XPS analysis was performed to ensure precise detection of the surface composition, Figure 4. In the expected binding energy of Ni(II), ~854, eV, no sufficient peak was observed. The atomic composition of 0.3% that was measured for the nickel cations, Table S1, indicates their low presence in the surface for this specimen of 1% Ni (II)@ORMOSIL. This value is close to the reported detection limit [28]. This result strengthens the notion that most of the catalytic activity exhibited by the nanocomposite catalyst is due to catalysis happening in the bulk of the material.
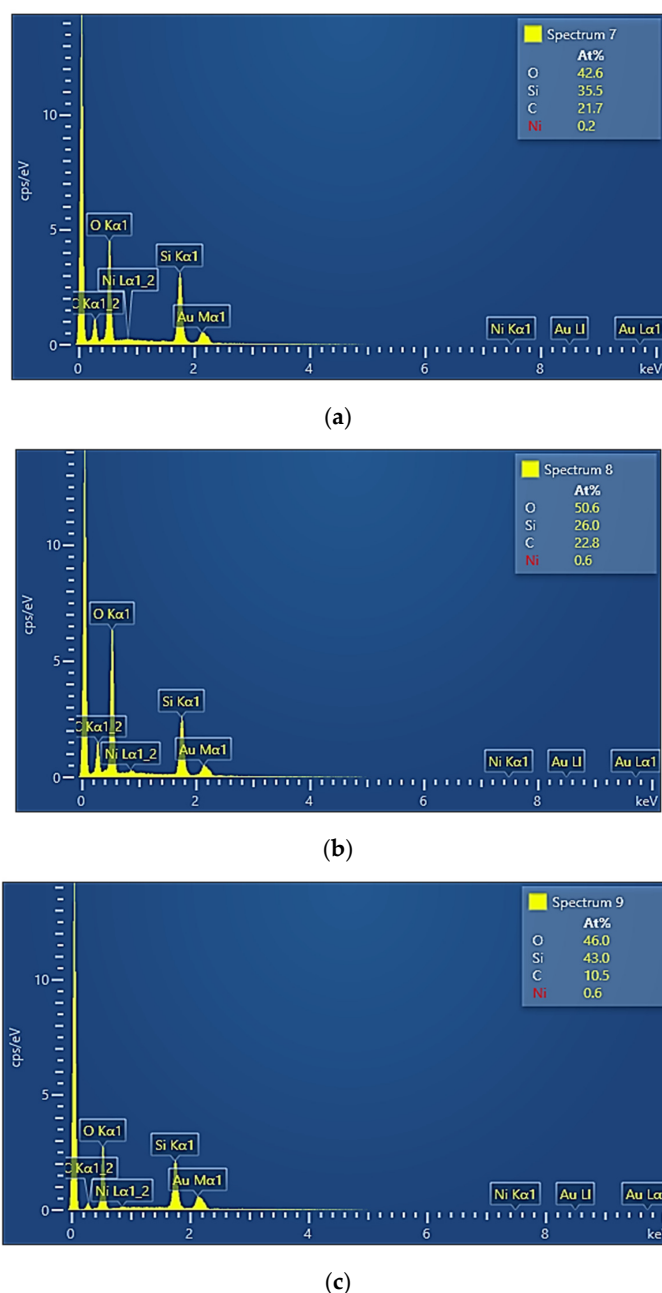
(**a**)

(**b**)

(**c**)

Figure 3. EDAX elemental composition spectra measured in the three areas marked in Figure 2: (**a**) spectrum 7; (**b**) spectrum 8; (**c**) spectrum 9.

The XRF emission spectra of 1% mol Ni(II)@ORMOSIL revealed the typical Kα1 at 7.48 KeV and Kβ1 at 8.26 Kev emissions, indicating sufficient nickel presence in the bulk of the material, Figure 5.

The incorporation of metal cation into the sol-gel silica matrix also results in a major effect on the siloxane ring sizes. This effect is a function of the cation charge density. Ni^{2+} has a relatively high charge density [29]. Divalent transition metal cations, Ni^{2+}, interact with surface silanols (Si-OH) and siloxane bridges (Si-O-Si). Incorporating divalent metal cations into the structure might lead to the formation of Ni(OH)$_2$ [29–31]. These phases may be identified by their typical diffraction patterns.

The use of highly saturated metal-ORMOSIL matrices for identifying the phases obtained is a valuable strategy to overcome difficulties in identifying the obtained metal phases due to shielding effects by the amorphous matrix. The diffractogram in Figure 6

of 10% mol loaded Ni(II)@ORMOSIL matrix revealed small and broad peaks of nickel silicate hydroxide hydrate ($Ni_3Si_4O_{10}(OH)_2 \cdot 5H_2O$) and nickel hydroxide($Ni(OH)_2$) phases, Table S2.
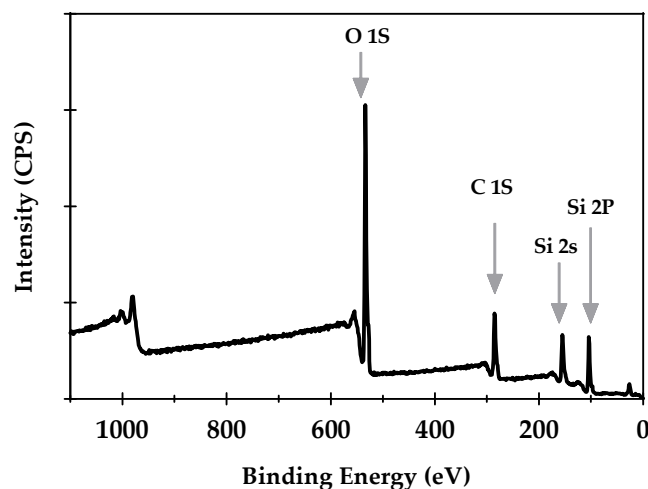

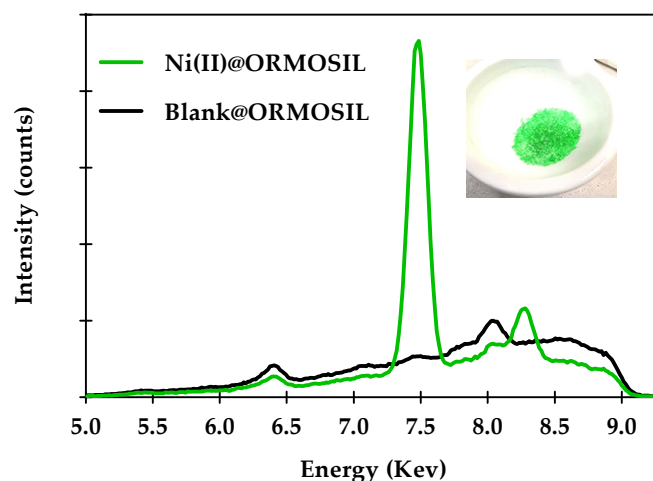**Figure 4.** XPS spectrum of 1.0% Ni (II)@ORMOSIL.

Figure 5. XRF spectra; Blank@ORMOSIL-black, Ni(II)@ORMOSIL-green, Inset: ground green Ni (II)@ORMOSIL.
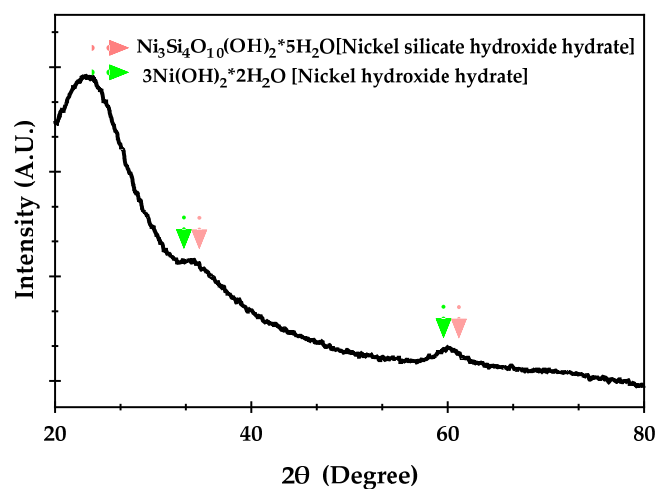

Figure 6. PXRD diffractogram; 10% Ni (II)@ORMOSIL.

Particle sizes were not calculated since Ni(II)@ORMOSIL is a pre-catalyst that serves as a precursor to obtain zero-valent nickel (ZVNi) nanoparticles during the reduction process with $NaBH_4$ that is used as the reducing agent for both the metal and the pollutant. This is an in-situ strategy of nanofabrication and environmental pollutant degradation applied by the Ni(II)@ORMOSIL pre-catalyst.

Ni(II)@ORMOSIL was used in the reduction of nitrobenzene with $NaBH_4$. The addition of $NaBH_4$ triggered a color change from the described green hue [21] to a typical black, Figure 7. This color change suggests the formation of zero-valent nickel particles, ZVNi, reaction (1). After the specified reaction time of 60 min, the black silica particles (ZVNi@ORMOSIL) were separated from the reaction suspension by vacuum filtration. The filtrate was separated and analyzed by HPLC, and the silica filter cake was washed and left to dry in a desiccator at ambient temperature.
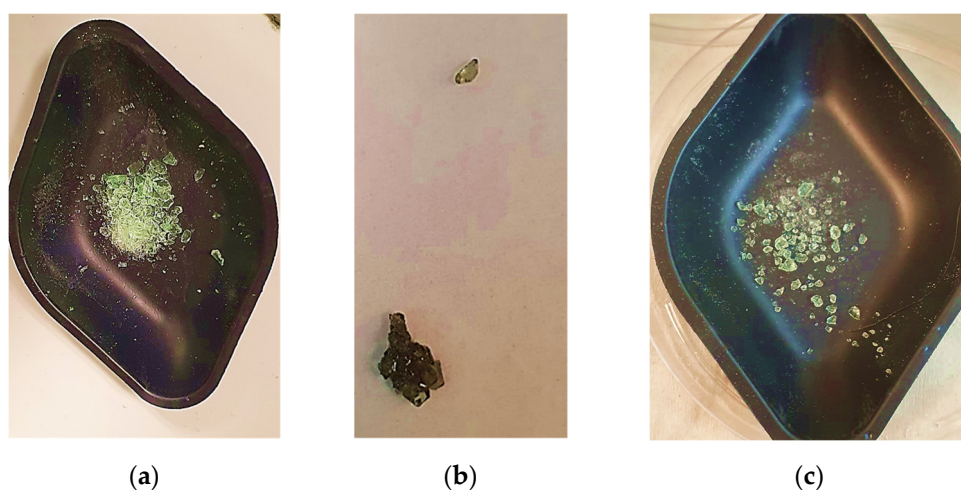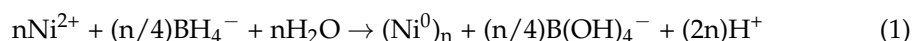
$$nNi^{2+} + (n/4)BH_4^- + nH_2O \rightarrow (Ni^0)_n + (n/4)B(OH)_4^- + (2n)H^+ \tag{1}$$

| (a) | (b) | (c) |

Figure 7. The process of the typical color change of Ni(II)@ORMOSIL undergoing the reduction of NB with $NaBH_4$ followed by oxidation to the initial green color in ambient conditions. (**a**) Ni(II)@ORMOSIL powder. (**b**) ZVNi@ORMOSIL filter cake, (**c**) same nickel matrix after washing and drying in ambient conditions.

After ~12 h, the obtained "black nickel" grafted in silica returned to the green hue described earlier, as shown in Figure 7c. It should be noted that the color change is gradual, and without washing with water in ambient conditions might take more time. The reversibility of green-black-green color changes implies the ZVNi@ORMOSIL formation and the following oxidation by washings with water. Identification of nickel silicate hydroxide hydrate and nickel hydroxide hydrate phases in the Ni(II)@ORMOSIL matrix is indicative of the metal catalyst presence and catalysis occurring in the bulk of the ORMOSIL matrix.

Attempts to obtain the diffraction of the "suspected" zero-valent nickel (ZVNi) nanoparticles matrix (black particles state) "ZVNi@ORMOSIL" were made (Figure S3). However, due to the significant excess of $NaBH_4$, only $Na_2B_4O_5(OH)_4 \cdot 8H_2O$ was detected (Table S3). In a similar case, sodium borax hydroxide hydrate was reported as a byproduct of $NaBH_4$ hydrolysis in the reduction of the metal chloride [32] to nanoparticles.

To verify the formation of ZVNi@ORMOSIL, the UV-Vis spectrum of the black ZVNi@ORMOSIL gel was measured and compared to the spectrum of the non-reduced, green-colored Ni(II)@ORMOSIL gel. The distinctive peak, at about 400 nm, characteristic of Ni(II), was not obtained for the black-colored "suspected" ZVNi@ORMOSIL, as shown in Figure S4. The disappearance of an absorption maximum that is typical for Ni^{2+} is indicative of an oxidation state change, in this case to Ni^0, as a result of the reduction with

$NaBH_4$. Similar evidence was reported earlier for Pt^0 formation as a result of K_2PtCl_4 reduction [33].

N_2 adsorption-desorption study was performed on Ni(II)@ORMOSIL before and after reduction, after sufficient washing and drying, to examine the possible effect of the reduction on the matrices pore volume and diameter. 1% Ni(II)@ORMOSIL exhibits adsorption/desorption isotherms forming hysteresis loop type H4, Figure 8, indicative of a narrow slit-like pore framework [34], which are reported for crystal zeolites and some mesoporous zeolites [35]. This is unlike the ink-bottle shaped pore of H2A type observed in nanoparticles hosting ORMOSIL matrices reported earlier [13] for the ZVI@ORMOSIL and seen in silica gels and porous glasses (Vycor) [35].
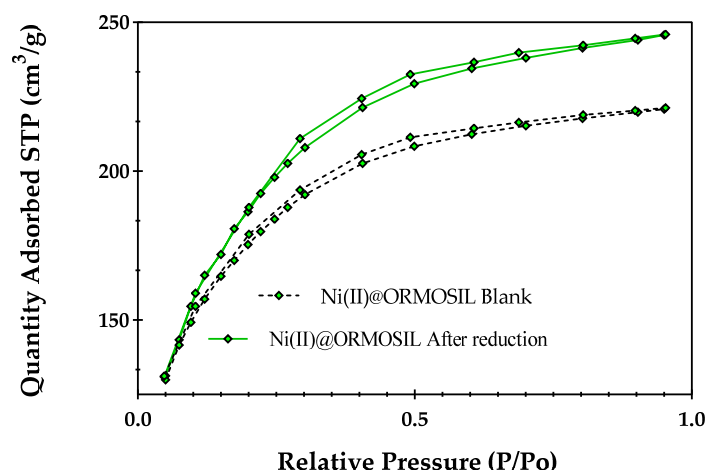

Figure 8. Adsorption-desorption isotherms of the unreduced 1% Ni(II)@ORMOSIL (dashed line) and reduced 1% Ni(II)@ORMOSIL (green line).

As summarized in Table 1, the nickel incorporated ORMOSIL matrices exhibited stability in retaining surface area, pore size, and volume of the Ni(II)@ORMOSIL matrix subjected to reaction conditions described in the experimental section. Proper washing and drying were performed before and after the treatment to ensure the appropriate comparison to the matrix that was not subjected to $NaBH_4$. The slight changes in the surface area induced by the redox cycling of the Ni(II)@ORMOSIL might be due to nanoparticle formation and further possible migration inside the silica voids [36], but might also be considered as a non-significant change. Only a slight increase in pore volume reduces the risk of pore-blocking [37], and the same pore diameter might indicate certain structure stability. In previous studies of Au^o and Ag^o nanoparticles incorporated into ORMOSIL matrices, Au-cat and Ag-cat, surface area analysis (BET) was obtained as 428 m^2/g and 452 m^2/g, respectively [28,38]. Silversil [39] catalyst composed of 70:30 mole ratio of tetraethoxysilane (TEOS) and methyltriethoxysilane (MTEOS) respectively, resulted in 583 m^2/g surface area. The surface area of these organically modified silica matrices (ORMOSIL) is highly dependent on their monomer ratio (under the same synthetic procedures) [39]. For ZVI@ORMOSIL the synthetic procedure included a 70:30 mole ratio of TEOS and methyltrimethoxysilane (MTMOS) as monomers, exhibiting a surface area of 751 m^2/g. Roughly, the surface area (m^2/g) obtained for $NiCl_2 \cdot 6H_2O$ grafted ORMOSIL (before and after reduction) is between the values obtained for Ag-cat, Au-cat [28,38], Silversil [39], and ZVI@ORMOSIL [12].

Table 1. N$_2$ Adsorption-Desorption isotherms summary.

Sample	BET Surface (m^2/g)	Average Pore Volume (cm^3/g)	Average Pore Diameter (nm)
Ni(II)@ORMOSIL no reduction	602	0.34	3.6
Ni(II)@ORMOSIL reduced and re-oxidized	660	0.38	3.6

2.2. Catalytic Reduction of Nitrobenzene

Figure 9 presents a schematic outline of the observed reaction process according to the product distribution obtained.
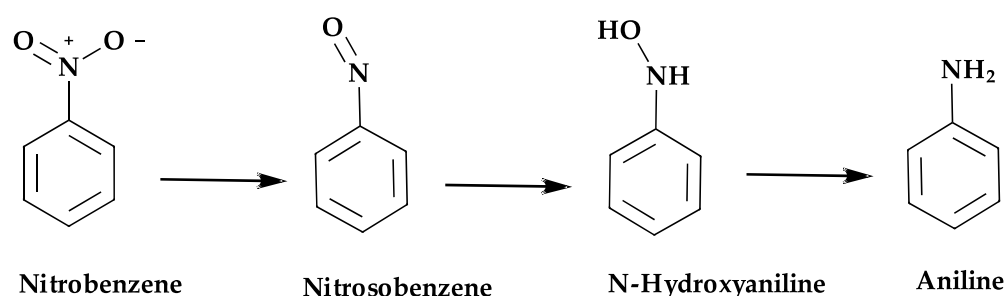

Figure 9. Reduction products of nitrobenzene (NB), nitrosobenzene (NOB), n-hydroxyaniline (PhN-HOH) and aniline (PhNH$_2$).

The reduction of nitrobenzene to aniline is a stepwise process going from nitrobenzene (NB) to nitrosobenzene (NOB), then to N-hydroxyaniline (PhNHOH), and finally to aniline [40]. This is considered the direct route to aniline. An alternative route to obtain aniline is via a condensation route, which is achieved by the condensation of NOB with PhNHOH [40]. NB reduction by ZVI as the reducing agent in aerobic media proceeds via the condensation route and results in azoxybenzene and azobenzene under oxygen-limited conditions [41]. ZVI-induced advanced oxidation of aniline yields azoxybenzene [41]. NB reduction with NaBH$_4$ catalyzed by ZVI@ORMOSIL inhibits that possibility for obvious reasons. NaBH$_4$ is added in molar access with respect to the NB initial concentration. The NB reduction to aniline requires six electrons per mole. The addition of more than a 1:1 mol ratio of SBH with respect to the initial NB amount yields a reducing agent excess. This excess is required as the catalytic reduction is always accompanied by H$_2$ evolution [42,43]. Furthermore, when the M^0-NPs are formed in situ, this also requires reduction capacity. Conversion of NB to aniline and NOB using Fe^0 powder as the reducing agent in anaerobic conditions without the formation of azobenzene or azoxybenzene being observed was attributed to an increase in BET surface area that induced an increase in the reduction rates [44]. Sol-gel entrapped ZVI catalysts have a high surface area [13]. Catalytic reductions, presented herein, are performed in water and acetonitrile mixtures of various compositions. Acetonitrile is a polar aprotic solvent previously used in NB reductions [16].

2.2.1. ZVI@ORMOSIL Catalyzed Reduction of Nitrobenzene with NaBH$_4$

Nitrobenzene was reduced in the presence of 1% ZVI@ORMOSIL catalyst, prepared by the reported procedure [13]. NaBH$_4$ enhances ZVI reactivity in oxygen environments by rejuvenating the passivated surface [45].

Nitrobenzene reduction with ZVI@ORMOSIL as a catalyst produced a significant yield of aniline, Figure 10. 90% Acetonitrile was used to provide sufficient organic solvent to homogenize the NB suspension and yet enough water for sufficient SBH hydrolysis. The reaction was monitored after 12 h since SBH mediated reductions in the acetonitrile-rich environment take more time for efficient transformation [13]. These conditions enabled 30% conversion to PhNHOH and 56% conversion to aniline, a very promising result that might be optimized by changing the catalyst to a different metal.
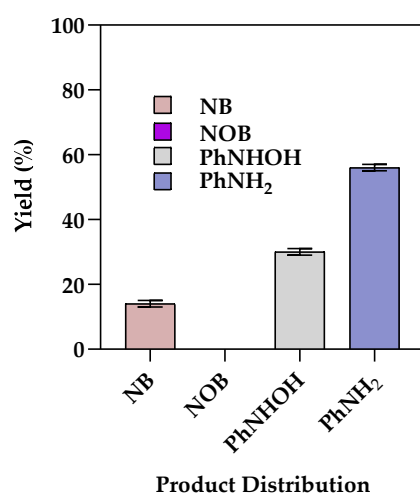
Figure 10. ZVI@ORMOSIL catalyzed reduction of NB. The reaction suspension contained 0.20 g ZVI@ORMOSIL at ambient conditions. Reaction time 12 h. 1.0 mM [NB], 60 mM [NaBH$_4$], reaction medium: 90% acetonitrile, 10% water.

2.2.2. 1.0%. Ni@ORMOSIL Reduction of Nitrobenzene

1.0%. Ni@ORMOSIL Nitrobenzene Reduction with NaBH$_4$ in Different Reaction Media

To examine the possibility of shorter reaction periods, with increased substrate concentration, it was decided to use a pre-catalyst loaded ORMOSIL matrix. NiCl$_2$ dissolved in homogeneous media was shown to be a pre-catalyst for the reduction of nitro-arenes by BH$_4^-$ [15,16]. It was therefore decided to study the effect of the ORMOSIL matrix on this catalytic process. Ni(II)@ORMOSIL, in various catalyst mol percent loads, were prepared (1.0%, 0.2%, 0.1%) and reacted as catalysts of the NB reduction with BH$_4^-$. The experiments with the 1% Ni(II)@ORMOSIL matrices were performed under conditions where the mole concentration of nickel was identical to that used in the homogeneous medium to assess the effect of the porous matrix on the catalytic efficiency. Figure 11 presents the reaction products of NB reduction by BH$_4^-$ with 1% mol Ni(II)@ORMOSIL as a catalyst in a different volumetric ratio of water and acetonitrile. The 98% conversion to aniline, obtained in 10% acetonitrile, Figure 11a, indicates that the reaction proceeds more efficiently in the aqueous-rich medium, probably due to the faster hydrolysis of NaBH$_4$. When the reaction was performed in a reaction medium of 90% acetonitrile, 92% conversion to aniline was obtained, Figure 11b. The intermediate products NOB and N-hydroxylaniline that desorb better in the medium with the lower dielectric constant were also detected with 4.0% and 2.0% yield, respectively. Identical observations were made with ZVI@ORMOSIL catalyzed chloroacetamides reductions in various media [13]. Hence, a change in the reaction media composition to 90% acetonitrile is a valuable study tool to observe other reduction products, otherwise consumed in a fast reaction cascade. Comparison of the results presented in Figures 10 and 11b indicates that the Ni(II)@ORMOSIL is a better catalyst.

0.2%. and 0.1% Ni(II)@ORMOSIL Reduction of Nitrobenzene with NaBH$_4$

An attempt to limit the catalyst loading was performed with 0.1% Ni(II)@ORMOSIL and 0.2% Ni(II)@ORMOSIL. Reductions were carried out at different NB:NaBH$_4$ mole ratios, and the results are presented in Figures 12 and S9. A complete conversion to aniline (100% conversion) was achieved. Surprisingly, reduction efficiency was the same at 1:10 mole ratio (substrate: NaBH$_4$) compared to experiments performed with a higher concentration of NaBH$_4$, with a complete transformation to aniline. Thus, the results clearly indicate that 1.9 μmol Ni(II) are enough to catalytically reduce 100 μmol NB within less than 60 min.
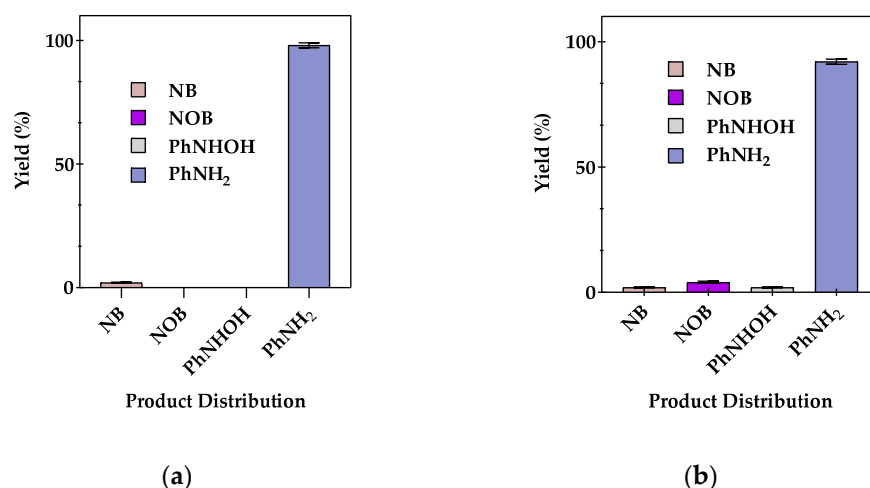
(**a**)

(**b**)

Figure 11. Product distribution of NB reduction performed in different reaction media. The reaction suspensions contained 0.20 g 1% Ni(II)@ORMOSIL catalyst at ambient conditions, 10 mM [NB], 60 mM [NaBH$_4$]. Reaction time 60 min, reaction medium: (**a**) 10% Acetonitrile, (**b**) 90% Acetonitrile.
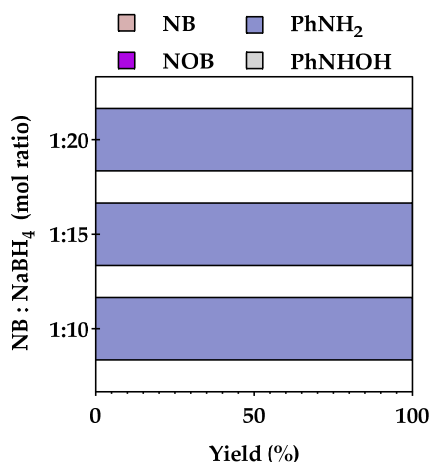

Figure 12. Product distribution of NB reduction, the catalyst load effect. The reaction suspensions contained 0.20 g 0.1% Ni(II)@ORMOSIL catalyst at ambient conditions. Reaction time 60 min. 10 mM [NB], 100, 150, 200 mM [NaBH$_4$], reaction medium: 10% Acetonitrile.

The catalyst efficiency, as a turnover number (TON) of about 53, was calculated for 0.1% Ni(II)@ORMOSIL, Equation (2). This value can be compared to silver nanoparticles in the TiO$_2$ matrix, catalyzing the reduction of nitroarenes, exhibiting a TON of 125. The loading was reported as 0.8% mol per catalytic support but with a lower NaBH$_4$ excess ratio of 1:8 [46]. Although the TON is almost half, the Ni(II)ORMOSIL introduces an important alternative for precious metals nanoparticles catalysts by using the earth-abundant and in-situ prepared nickel pre-catalyst.

$$\text{TON (turnover number)} = \frac{\text{Total moles of reacted substrate}}{\text{Total moles of the catalyst}} \qquad (2)$$

NiCl$_2$ as a Catalyst for the Reduction of NB by NaBH$_4$ in Homogeneous Media

Ni$^{2+}_{\text{aq}}$ is known to catalyze the reduction of nitroarenes by NaBH$_4$ in homogeneous media [15,16]. It seemed of interest to compare the catalytic properties of Ni(II)@ORMOSIL with those of Ni$^{2+}_{\text{aq}}$. For this purpose, the catalytic properties of Ni$^{2+}_{\text{aq}}$ were studied under identical conditions to those used for the heterogeneous experiments, i.e., the same solution composition and the same amount of Ni(II) ions, 19 μmol. The results are presented in Figure 13. An increase in the NaBH$_4$ ratio could not achieve a notable increase in the

conversion to aniline. However, total consumption of NB was visible in the gradual decrease of NB in the reaction solution from 52% to 42%, 23%, and 0% for the NB: NaBH$_4$ mole ratios of 1:6, 1:10, 1:15, and 1:20, respectively (Figure 13a). Interestingly, no apparent change was noted for the 90% acetonitrile media. As the mole ratio increased from 1:6 to 1:10, only a 6% increase was obtained in the conversion of NB, i.e., increasing from 27% to 33%, finally obtaining only 22% yield of PhNHOH and 11% yield of aniline (Figure 13b).
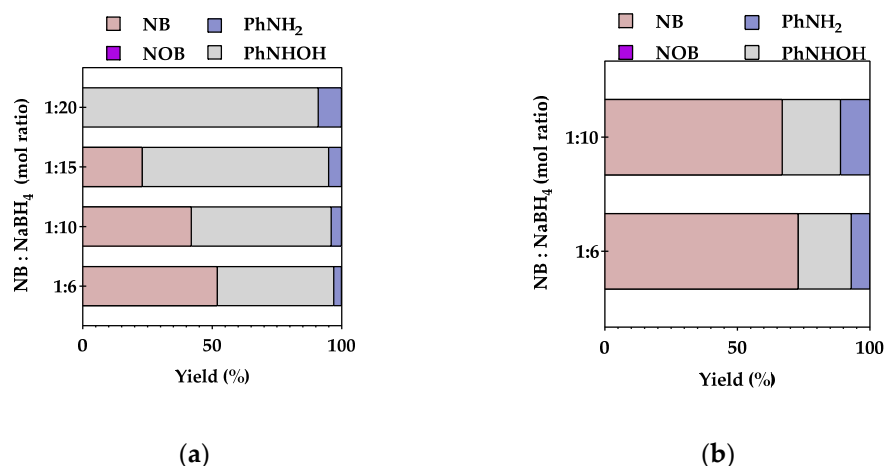

(a)　　　　　　　　　　　　　　　　　　　(b)

Figure 13. Effect of [NaBH$_4$] on the product distribution. The reaction solution contained 19 μmol NiCl$_2$·6H$_2$O (equivalent to 0.2 g 1%Ni(II)@ORMOSIL) at ambient conditions. Reaction time 60 min. 10 mM [NB], (**a**) 60, 100, 150, 200 mM [NaBH$_4$], (pH$_0$ = 5.9, pH$_f$ = 10.6). (**b**) 60, 100 mM [NaBH$_4$], reaction medium: (**a**) 10% acetonitrile, (**b**) 90% acetonitrile.
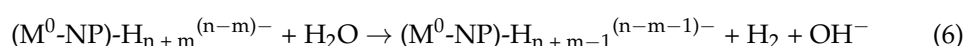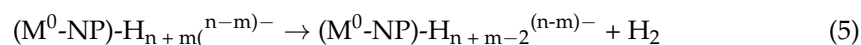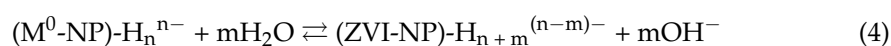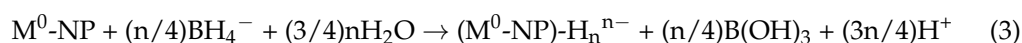
A comparison of the results with those presented in Figure 11, clearly points out that the Ni(II)@ORMOSIL is a considerably better catalyst than Ni$^{2+}_{aq}$. Furthermore, the results indicate that the catalytic reduction of NOB is much easier than that of NB as no NOB is observed though NB is still available. The results also suggest that PhNHOH is more difficult to reduce than NB. It is of interest to note that the color of the solutions, even in the presence of a large excess of BH$_4^-$, did not change to black.
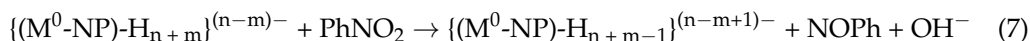
2.2.2.4. 1%. Ni(II)@ORMOSIL Catalyst Stability

Catalyst re-usability was tested by performing three consecutive catalytic cycles, Figure S10, with repeated washing and drying after each cycle. The overall yields remained unchanged, indicating that the Ni(II)@ORMOSIL matrices are stable.
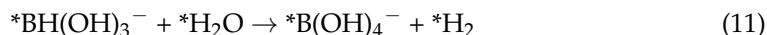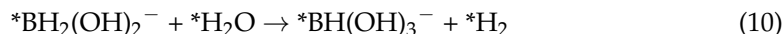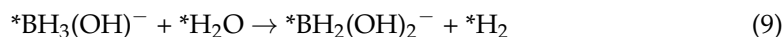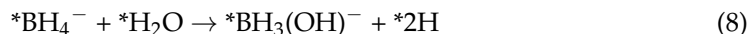
2.2.3. Mechanistic Analysis of NB Reduction

The observation that the Ni(II)@ORMOSIL pre-catalyst turns black during the catalytic process may suggest that Ni^0-NPs-ORMOSIL is the actual catalyst. Therefore, the catalytic reductions in the presence of ZVI-ORMOSIL and Ni(II)@ORMOSIL are discussed for M^0-ORMOSIL. It is commonly assumed that the catalyzed hydrolysis of BH$_4^-$ on M^0-surfaces proceeds via reactions (3) and (4) [45] that in the absence of an oxidizing substrate will be followed by H$_2$ evolution via reactions (5) and/or (6) [47]. In the presence of an oxidizing substrate, e.g., NB, reaction (7) assuming a hydride transfer, will compete with reactions (5) and (6). If the reduction proceeds via an H atom transfer, the first product will naturally be a radical.

$$M^0\text{-NP} + (n/4)BH_4^- + (3/4)nH_2O \rightarrow (M^0\text{-NP})\text{-H}_n^{n-} + (n/4)B(OH)_3 + (3n/4)H^+ \quad (3)$$

$$(M^0\text{-NP})\text{-H}_n^{n-} + mH_2O \rightleftarrows (ZVI\text{-NP})\text{-H}_{n+m}^{(n-m)-} + mOH^- \quad (4)$$

$$(M^0\text{-NP})\text{-H}_{n+m(}^{n-m)-} \rightarrow (M^0\text{-NP})\text{-H}_{n+m-2}^{(n-m)-} + H_2 \quad (5)$$

$$(M^0\text{-NP})\text{-H}_{n+m}^{(n-m)-} + H_2O \rightarrow (M^0\text{-NP})\text{-H}_{n+m-1}^{(n-m-1)-} + H_2 + OH^- \quad (6)$$

$$\{(M^0\text{-NP})\text{-H}_{n+m}\}^{(n-m)-} + PhNO_2 \rightarrow \{(M^0\text{-NP})\text{-H}_{n+m-1}\}^{(n-m+1)-} + NOPh + OH^- \quad (7)$$

However, for the hydrolysis of BH_4^- on Ag^0, recent DFT calculations [48] indicate that the mechanism involves the following reactions: (* signifies an adsorbed species.)

$$*BH_4^- + *H_2O \rightarrow *BH_3(OH)^- + *2H \quad (8)$$

$$*BH_3(OH)^- + *H_2O \rightarrow *BH_2(OH)_2^- + *H_2 \quad (9)$$

$$*BH_2(OH)_2^- + *H_2O \rightarrow *BH(OH)_3^- + *H_2 \quad (10)$$

$$*BH(OH)_3^- + *H_2O \rightarrow *B(OH)_4^- + *H_2 \quad (11)$$

If this mechanism is general, only two H· atoms, one of them stemming from water, are adsorbed on the M^0-NPs, and the rest of the H_2 is formed without the involvement of adsorbed hydrogen atoms or hydrides. Furthermore, when H· atoms are adsorbed on the silver, reaction (8) is replaced by reaction (12). This means that the mechanisms of H_2 evolution and substrates reductions must be reconsidered; i.e., adsorbed BH_4^- might be the reducing agent.
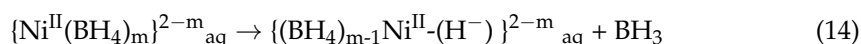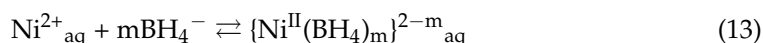
$$*BH_4^- + *H_2O \rightarrow *BH_3(OH)^- + *H_2 \quad (12)$$
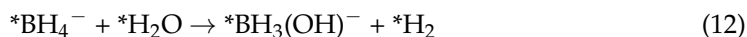
Catalytic Reductions by M^0

The experimental results for the catalytic H_2 evolution on Ag^0 [49] are in agreement with reactions (8)–(12). However, the results for the catalytic H_2 evolution on Au^0 [49] clearly indicate a different mechanism.
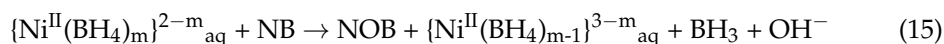
These derivations point out that the hydrolysis mechanism depends on the adsorption energies of BH_4^- and H· on the metal. Clearly, therefore DFT calculations for Fe^0 and Ni^0 must be performed prior to drawing conclusions about the mechanisms of the reactions studied.

Catalytic Reductions by Ni^{2+}_{aq}

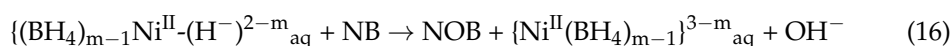As the redox potential of the couple, Ni^{2+}_{aq}/Ni^0 atom in aqueous solutions is -2.24 V vs. SHE [50], clearly, some intermediates must be formed prior to the formation of Ni^0_{solid}. As the solutions did not turn black during the catalytic cycles, the NB is probably reduced by these intermediates. The most plausible intermediates are $\{Ni^{II}(BH_4)_m\}^{2-m}{}_{aq}$ or $Ni^{II}(H)^+{}_{aq}$ formed via:

$$Ni^{2+}_{aq} + mBH_4^- \rightleftarrows \{Ni^{II}(BH_4)_m\}^{2-m}{}_{aq} \quad (13)$$

$$\{Ni^{II}(BH_4)_m\}^{2-m}{}_{aq} \rightarrow \{(BH_4)_{m-1}Ni^{II}\text{-}(H^-)\}^{2-m}{}_{aq} + BH_3 \quad (14)$$

or some aggregates of these species. These will then reduce the substrate, e.g., NB via a hydride transfer:

$$\{Ni^{II}(BH_4)_m\}^{2-m}{}_{aq} + NB \rightarrow NOB + \{Ni^{II}(BH_4)_{m-1}\}^{3-m}{}_{aq} + BH_3 + OH^- \quad (15)$$

Or

$$\{(BH_4)_{m-1}Ni^{II}\text{-}(H^-)^{2-m}{}_{aq} + NB \rightarrow NOB + \{Ni^{II}(BH_4)_{m-1}\}^{3-m}{}_{aq} + OH^- \quad (16)$$

3. Materials and Methods

3.1. Materials

Tetraethyl orthosilicate (TEOS) $\geq$99.0%, methyltrimethoxysilane (MTMOS) $\geq$99.0%, and ZVI 25 nm powder 99.5% were purchased from Sigma Aldrich (Sigma-Aldrich, Rehovot, Israel). $NaBH_4$ 98% was purchased from Acros (Thermo Fischer Scientific, Geel, Belgium). Hydrochloric acid (HCl, 37%), HPLC grade 85% H_3PO_4, and 25% NH_3 (as NH_4OH) were purchased from Merck (Merck, Darmstadt, Germany). $NiCl_2 \cdot 6H_2O$ (>98), nitrobenzene (NB) 99%, and aniline 99+% were purchased from Alfa Aesar (Alfa Aesar, Beijing, China). Nitrosobenzene (NOB) 98.0%, N-phenylhydroxylamine (PhNHOH) 97% were purchased from Angene (Angene International Limited, London, England). LCMS

grade solvents: ethanol and acetonitrile were purchased from Bio Lab Ltd (BIO-LAB LTD., Jerusalem, Israel). All chemicals were of A.R. grade and were used as received. All aqueous solutions were prepared from deionized water purified by a Millipore Milli-Q set up (Merck, Darmstadt, Germany) with a final resistivity of >10 MΩ/cm.

3.2. Catalyst Preparation

3.2.1. 1.0%. mol Loading of ZVI@ORMOSIL

The catalyst was prepared by using the two-steps acid/base sol-gel synthesis route. Briefly, 37% HCl (62 μL, 2.02 mmol) was dissolved in water (2.72 g, 0.151 mol), and the mixture was added slowly into a pre-mixed solution containing MTMOS (1.556 g, 0.011 mol) and TEOS (5.6 g, 0.027 mol), that were dissolved in ethanol (7.02 g, 0.152 mol). The resulting mixture was homogenized for 15 min. 2.0% NH_3 solution (1.5 mL, 7.7 mmol) was then added to the mixture dropwise. When the gelation started, 380 μL of 1.0 M ethanolic suspension of ZVI was added, and the mixture was stirred vigorously. The wet black gel was kept for 15 days for aging and drying at room temperature. The solid matrix obtained was crushed with mortar and pestle into a powder and washed with water several times. The washed matrix was then dried and used for the catalytic tests.

3.2.2. 1.0%. mol Loading of Ni(II)@ORMOSIL Pre-Catalyst

The catalyst was prepared by using the two-steps acid/base sol-gel synthesis route. Briefly, 37% HCl (62 μL, 2.02 mmol) was dissolved in water (2.72 g, 0.151 mol). The mixture was added slowly into a pre-mixed solution containing MTMOS (1.556 g, 0.011 mol) and TEOS (5.6 g, 0.027 mol) that were dissolved in ethanol (7.02 g, 0.152 mol). The resulting mixture was homogenized for 15 min. $NiCl_2 \cdot 6H_2O$ (0.090 g, 0.38 mmol) was added to the solution and homogenized for another 15 min. 2.0% NH_3 solution (1.5 mL, 7.7 mmol) was added to facilitate gelation. The wet green gel was kept for 15 days for aging and drying at room temperature. The solid matrix obtained was crushed with mortar and pestle into a powder and washed with water several times. The washed matrix was then dried and used for the catalytic tests. The pre-catalysts containing 0.1%, 0.2%, and 10% of Ni(II) were prepared via identical procedures changing only the amount of $NiCl_2 \cdot 6H_2O$ added during the synthesis.

3.3. Catalyst Characterization

Transmission microscope image, electron microscopy, and the elemental composition were measured using a 3FE-Tescan ultra-high-resolution MAIA microscope with an AZTEC microanalysis EDX detector, Oxford Instruments, (Colorado, CO, USA). X-ray diffraction (XRD) measurements were performed with a Bruker (Karlsruhe, Germany) AXS D8 ADVANCE Series II diffractometer equipped with a LynxEye detector (reflection θ–θ geometry, Cu Kα radiation (λ = 0.154 nm), divergence slit 0.60 mm, anti-scattering slit 8.0 mm). Diffraction data were collected in the angular range of 20° < 2θ < 80°, step size 0.02° and a step time of 1.0 sec/step. N_2 adsorption-desorption isotherms were measured using an APP gold instruments VSorb 2800 model surface area and porosity analyzer, sensitivity 0.010 m^2/g, range 2–500 nm pore size. Specific surface area, average pore size distribution (PSD), pore-volume, and adsorption-desorption isotherms were evaluated using the Brunauer−Emmett−Teller (BET) and Barrett−Joyner− Halenda (BJH) methods. XPS surface analysis was performed using Thermo Fisher Scientific (East Grinstead, UK), NEXSA XPS system with monochromatized Al Kα source (400-micron diameter), Pass Energy ("resolution") of 200 eV was used for survey scans to obtain the general surface composition profile and 50 eV for the high-resolution scans that were used for quantitative analysis. The metal loading of the samples was measured on a Portable X-ray Fluorescence (pXRF), Niton XL3t GOLDD+ XRF analyzer instrument (Thermo Fisher Scientific, Waltham, MA, USA) with a silver (Ag) anode.

Spectrophotometric analysis. Absorbance spectra were collected in 1.0 cm quartz cuvettes, using Varian Cary UV Bio 50 (Varian Australia Pty Ltd, Mulgrave, Australia)

spectrophotometer with dual-beam, Czerny-Turner monochromator; a Xenon pulse lamp single source, dual Si diode detectors were used.

3.4. Catalytic Tests

3.4.1. Nitrobenzene Reductions with 1% ZVI@ORMOSIL

In a typical experiment, an amount of ZVI@ORMOSIL was weighed (ca. 0.20 g) in a glass vial, and 1.0 mL of 0.010 M NB (acetonitrile solution) was accurately transferred to the vial, 7.0 mL of acetonitrile and 0.023 g of SBH (0. 61 mmol SBH/0.010 mmol of the substrate) were added. Finally, adding 2.0 mL of de-aerated water to make up the total reaction volume to 10.0 mL, the resulting suspensions were stirred for 12 h. The catalyst was recovered by filtration, and the filtrate was analyzed by HPLC.

In blank experiments performed with a blank matrix (Blank@ORMOSIL) containing no metal incorporated into the ORMOSIL matrix prepared with the same composition, no reduction of NB was observed.

3.4.2. Nitrobenzene Reductions with 1%, 0.2% and 0.1% Ni(II)@ORMOSIL

Nitrobenzene was taken as a probe compound to study the catalytic activity of Ni(II)@ORMOSIL towards reduction. In a typical set of reduction experiments, Ni(II)@-ORMOSIL was weighed (ca. 0.20 g) in a glass vial, 8 mL of a solvent (de-aerated water, or acetonitrile) was added,1.0 mL of 0.10 M nitrobenzene (acetonitrile solution) was transferred, 0.023 g of $NaBH_4$ were accurately added to the vessel with a relative excess ratio of 1:6 (0.10 mmol of substrate/0.61 mmol $NaBH_4$). Finally, 1.0 mL of de-aerated water was added to complete a total reaction volume of 10.0 mL. In the second set of reduction experiments, the initial amount of water was replaced with the same volume of acetonitrile, thus obtaining (9:1) (acetonitrile: water) suspension. The resulting solutions were stirred for 60 min. After that, the catalyst was recovered by filtration, and the filtrate was analyzed by HPLC. A representative chromatogram is depicted in Figure S11.

3.4.3. Nitrobenzene Homogenous Reductions with $NiCl_2 \cdot 6H_2O$

$NiCl_2 \cdot 6H_2O$ solutions containing amounts of nickel ions equivalent to the 1% Ni(II)@-ORMOSIL experiments were transferred to a glass vial. 3.0 mL of (de-aerated water, or acetonitrile) to which was added 1.0 mL of 0.10 M nitrobenzene and 0.023 g of $NaBH_4$ finally, 1.0 mL of de-aerated water was added to complete a total reaction volume of 10.0 mL.

The resulting solutions were stirred for 60 min. Then, the reaction solutions were analyzed by HPLC.

The catalyst performance in the NB reduction was monitored by HPLC analysis and evaluated by calculating the yield percent (Yield (%)). The formula is given in Equation (17). The standard calibration curves for NB, NOB, PhNHOH, and aniline, obtained by linear regression, are presented in Figure S12. The chromatograms obtained for the standards solutions are shown in Figure S13. The Standards stock solutions were prepared freshly in the same manner as a sample reaction solution but were not exposed to the reducing agent. The percent yield as presented in Equation (17) accounts for the peak areas as obtained in the HPLC analysis. In the case of the residual NB, the obtained peak area is considered as yield % for the uniformity of the discussion.

$$\text{Yield } (\%) = \left(\frac{\text{Sample area } \times \text{ Conc. of the standard}}{\text{Standard area}} \right) / (\text{Theoretic conc.}) \times 100 \qquad (17)$$

HPLC analysis was performed on a Dionex Ultimate 3000 equipped with Diode Array Detector by Thermo (Germering, Germany), Hypersil-gold C18 150*4.6 mm 3 μm column. Nitrobenzene, Nitrosobenzene, N-Phenylhydroxylamine, and aniline were eluted with (0.10% H_3PO_4; ACN), (60:40) mobile phase, 0.7 mL/min flow, 27 °C column temp, with UV detection at 200 nm, 10 μL injection volume. The reaction samples were quenched with a few drops of diluted H_3PO_4, filtered through 0.22 μm PES or H-PTFE according to the

reaction solvent. The reaction samples, standards, and blanks were diluted and adjusted to pH 3.0, filtered with 0.22 μm PES filter membrane before RP-HPLC monitoring for the degradation of nitroarenes.

NB, NOB, PhNHOH, and PhNH$_2$ standard stock solutions of 1000 μg/mL were prepared by accurately weighing or diluting adequate amounts and dissolving them in 30.0 mL acetonitrile. Working standards concentrations of 1, 2, 5, 10, 12.5 μg/mL and 25, 50, 75, 100, 120 μg/mL were prepared by dilution of the stock solution with de-aerated water to obtain calibration curves for HPLC quantifications of reaction conversions.

4. Conclusions

The results obtained in this study indicate that nickel ion-exchanged ORMOSIL matrices are efficient pre-catalysts for the catalytic reduction of NB to aniline by BH$_4{}^-$, even in aqueous media. These matrices are considerably more efficient than ZVI entrapped in an ORMOSIL matrix. Very low concentrations of nickel in the matrix are enough to form an efficient catalyst. The formation of black matrices during the catalytic process may suggest that Ni^0-NPs-ORMOSIL matrices that are unstable in the presence of O$_2$ are the actual catalysts. As the Ni^0-NPs-ORMOSIL matrices are unstable, it was impossible to determine whether the interaction between the nickel nanoparticles and the silica affects the catalytic properties. Such interactions were shown to affect other M^0-ORMOSIL catalyzed processes [51].

The fact that no NOB was observed suggests that Ni(II)@ORMOSIL is a better catalyst for the reduction of NOB than NB. The observation that PhNHOH is formed indicates that either it is more difficult to reduce PhNHOH than NB and/or that PhNHOH is desorbed from the catalyst surface. Also, no azoxybenzene or azobenzene was observed in analogy to observations on ZVI [52]. These results indicate that the mechanism does not involve the condensation route [37].

The excellent catalytic properties of the pre-catalyst Ni(II)@ORMOSIL are attributed to the homogeneous distribution of the nickel cations in the ion-exchanged matrix. Upon reduction, this allows obtaining small Ni^0-NPs, thus enabling better catalytic performances.

References

1. Ju, K.S.; Parales, R.E. Nitroaromatic Compounds, from Synthesis to Biodegradation. *Microbiol. Mol. Biol. Rev.* **2010**, *74*, 250–272. [CrossRef]
2. Arora, P.K.; Bae, H. Toxicity and Microbial Degradation of Nitrobenzene, Monochloronitrobenzenes, Polynitrobenzenes, and Pentachloronitrobenzene. *J. Chem.* **2014**, *2014*, 265140. [CrossRef]
3. Zhao, Q.J.; Hsu, C.H. Nitrobenzene. In *Encyclopedia of Toxicology*, 3rd ed.; Wexler, P., Ed.; Academic Press: Cambridge, MA, USA, 2014; pp. 536–539. [CrossRef]
4. World Health Organization. *Guidelines for Drinking-Water Quality*, 4th ed. 1st Add. 2017. ISBN 9789241549950. Available online: https://apps.who.int/iris/handle/10665/254637 (accessed on 8 March 2021).
5. Guy, R.C. Nitrobenzene. In *Encyclopedia of Toxicology*, 2nd ed.; Wexler, P., Ed.; Elsevier: Amsterdam, The Netherlands, 2005; pp. 236–238. [CrossRef]
6. Cave, M.; Falkner, K.C.; McClain, C. Occupational and Environmental Hepatotoxicity. In *Zakim and Boyer's Hepatology*, 6th ed.; Sanyal, A., Ed.; Elsevier: Amsterdam, The Netherlands, 2012; pp. 476–492. [CrossRef]
7. Wu, L. Dilemmas downstream from the Songhua River spill. *J. Med. Toxicol.* **2006**, *2*, 112–113. [CrossRef]
8. Zhao, Y.; Lin, L.; Hong, M. Nitrobenzene contamination of groundwater in a petrochemical industry site. *Front. Environ. Sci. Eng.* **2019**, *13*, 29. [CrossRef]
9. Zhang, W.; Chen, L.; Chen, H.; Xia, S.Q. The effect of $Fe^0/Fe^{2+}/Fe^{3+}$ on nitrobenzene degradation in the anaerobic sludge. *J. Hazard. Mater.* **2007**, *143*, 57–64. [CrossRef]
10. Zhang, D.; Shen, J.; Shi, H.; Su, G.; Jiang, X.; Li, J.; Liu, X.; Mu, Y.; Wang, L. Substantially enhanced anaerobic reduction of nitrobenzene by biochar stabilized sulfide-modified nanoscale zero-valent iron: Process and mechanisms. *Environ. Int.* **2019**, *131*, 105020. [CrossRef]
11. Huang, Y.H.; Zhang, T.C. Reduction of nitrobenzene and formation of corrosion coatings in zerovalent iron systems. *Water Res.* **2006**, *40*, 3075–3082. [CrossRef] [PubMed]
12. Meyerstein, D.; Adhikary, J.; Burg, A.; Shamir, D.; Albo, Y. Zero-valent iron nanoparticles entrapped in SiO_2 sol-gel matrices: A catalyst for the reduction of several pollutants. *Catal. Commun.* **2019**, *133*, 105819. [CrossRef]
13. Meistelman, M.; Meyerstein, D.; Bardea, A.; Burg, A.; Shamir, D.; Albo, Y. Reductive Dechlorination of Chloroacetamides with $NaBH_4$ Catalyzed by Zero Valent Iron, ZVI, Nanoparticles in ORMOSIL Matrices Prepared via the Sol-Gel Route. *Catalysts* **2020**, *10*, 986. [CrossRef]
14. Pasinszki, T.; Krebsz, M. Synthesis and Application of Zero-Valent Iron Nanoparticles in Water Treatment, Environmental Remediation, Catalysis, and Their Biological Effects. *Nanomaterials* **2020**, *10*, 917. [CrossRef]
15. Setamdideh, D.; Khezri, B. Rapid and Efficient Reduction of Nitroarenes to Their Corresponding Amines with Promotion of $NaBH_4/NiCl_2 \cdot 6H_2O$ System in Aqueous CH_3CN. *Chem. Asian J.* **2010**, *22*, 5575–5580.
16. Zeynizadeh, B.; Sorkhabi, S. Fast and efficient protocol for solvent-free reduction of nitro compounds to amines with $NaBH_4$ in the presence of Bis-thiourea complexes of bivalent cobalt nickel, copper and zinc chlorides. *J. Chem. Soc. Pak.* **2016**, *38*, 679–684.
17. Wasiak, T.; Przypis, L.; Walczak, K.Z.; Janas, D. Nickel Nanowires: Synthesis, Characterization and Application as Effective Catalysts for the Reduction of Nitroarenes. *Catalysts* **2018**, *8*, 566. [CrossRef]
18. Ibraheem, H.H.; El-Mekkaw, D.M.; Hassan, S.A.; Selim, M.M. Innovative Method for the Reduction of Nitrophenols Using Nickel Nanocatalysts in Zeolite-Y Prepared from Egyptian Kaolin. *Egypt. J. Chem.* **2010**, *53*, 565–579. [CrossRef]
19. Feng, J.; Wang, Q.; Fan, D.; Ma, L.; Jiang, D.; Xie, J.; Zhu, J. Nickel-based xerogel catalysts: Synthesis via fast sol-gel method and application in catalytic hydrogenation of p-nitrophenol to p-aminophenol. *Appl. Surf. Sci.* **2016**, *382*, 135–143. [CrossRef]
20. Burg, A.; Wolfer, Y.; Shamir, D.; Kornweitz, H.; Albo, Y.; Maimon, E. Meyerstein The role of carbonate in electro-catalytic water oxidation by using Ni(1,4,8,11-tetraazacyclotetradecane)$^{2+}$ D. *Dalton Trans.* **2017**, *46*, 10774–10779. [CrossRef]
21. Adhikary, J.; Meyerstein, D.; Marks, V.; Meistelman, M.; Gershinsky, G.; Burg, A.; Shamir, D.; Kornweitz, H.; Albo, Y. Sol-gel entrapped Au^0- and Ag^0-nanoparticles catalyze reductive de-halogenation of halo-organic compounds by $BH_4{}^-$. *Appl. Catal. B* **2018**, *239*, 450–462. [CrossRef]
22. Basha, M.A.F. Optical properties and colorimetry of gelatine gels prepared in different saline solutions. *J. Adv. Res.* **2018**, *16*, 55–65. [CrossRef] [PubMed]
23. Mack, H.; Reisfeld, R.; Avnir, D. Fluorescence of rare earth ions adsorbed on porous vycor glass. *Chem. Phys. Lett.* **1983**, *99*, 238–239. [CrossRef]
24. Levy, D.; Reisfeld, R.; Avnir, D. Fluorescence of europium(III) trapped in silica gel-glass as a probe for cation binding and for changes in cage symmetry during gel dehydration. *Chem. Phys. Lett.* **1984**, *109*, 593–597. [CrossRef]
25. Wezynfeld, N.; Goch, E.W.; Bal, W.; Fraczyk, T. cis-Urocanic acid as a potential nickel(ii) binding molecule in the human skin. *Dalton Trans.* **2014**, *43*, 3196–3201. [CrossRef] [PubMed]
26. Takahashi, R.; Sato, S.; Sodesawa, T.; Kamomae, Y. Measurement of the diffusion coefficient of nickel nitrate in wet silica gel using UV/VIS spectroscope equipped with a flow cell. *Phys. Chem. Chem. Phys.* **2000**, *2*, 1199–1204. [CrossRef]
27. Hantsche, H. Comparison of basic principles of the surface-specific analytical methods: AES/SAM, ESCA (XPS), SIMS, and ISS with X-ray microanalysis, and some applications in research and industry. *Scanning* **1989**, *11*, 257–280. [CrossRef]
28. Shard, A.G. Detection limits in XPS for more than 6000 binary systems using Al and Mg Kα X-rays. *Surf. Interface Anal.* **2014**, *46*, 175–185. [CrossRef]

29. Das, U.; Zhang, G.; Hu, B.; Hock, A.S.; Redfern, P.C.; Miller, J.T.; Curtiss, L.A. Effect of Siloxane Ring Strain and Cation Charge Density on the Formation of Coordinately Unsaturated Metal Sites on Silica: Insights from Density Functional Theory (DFT) Studies. *ACS Catal.* **2015**, *5*, 7177–7185. [CrossRef]

30. Nimir, H.I.; Hamza, A.; Ibnelwaleed, A.H. Development of Greener D-Metal Inorganic Crosslinkers for Polymeric Gels Used in Water Control in Oil and Gas Applications. *Energies* **2020**, *13*, 4262. [CrossRef]

31. Livage, J.; Henry, M.; Sanchez, C. Sol-gel chemistry of transition metal oxides. *Prog. Solid. State Chem.* **1988**, *18*, 259–341. [CrossRef]

32. Hannauer, J.; Demirci, U.B.; Geantet, C.; Herrmann, J.M.; Miele, P. Enhanced hydrogen release by catalyzed hydrolysis of sodium borohydride–ammonia borane mixtures: A solution-state 11B NMR study. *Phys. Chem. Chem. Phys.* **2011**, *13*, 3809–3818. [CrossRef] [PubMed]

33. Vijay, A.K.; Meyerstein, D.; Marks, V.; Albo, Y. Kinetics of the reaction of H_2 with Pt^0-nanoparticles in aqueous suspensions monitored by the catalytic reduction of $PW_{12}O_{40}{}^{3-}$. *Inorg. Chem. Front.* **2021**, *8*, 989–995. [CrossRef]

34. Tang, X.; Jiang, Z.; Li, Z.; Gao, Z.; Bai, Y.; Zhao, S.; Feng, J. The effect of the variation in material composition on the heterogeneous pore structure of high-maturity shale of the Silurian Longmaxi formation in the southeastern Sichuan Basin, China. *J. Nat. Gas Sci. Eng.* **2015**, *23*, 464–473. [CrossRef]

35. Thommes, M.; Kaneko, K.; Neimark, A.V.; Olivier, J.P.; Rodriguez-Reinoso, F.; Rouquerol, J.; Sing, K.S.W. Physisorption of gases, with special reference to the evaluation of surface area and pore size distribution. *Pure Appl. Chem.* **2015**, *87*, 1–19. [CrossRef]

36. Hansen, T.W.; DeLaRiva, A.T.; Challa, S.R.; Datye, A.K. Sintering of Catalytic Nanoparticles: Particle Migration or Ostwald Ripening? *Acc. Chem. Res.* **2013**, *46*, 1720–1730. [CrossRef]

37. Jeromenok, J.; Weber, J. Restricted Access: On the Nature of Adsorption/Desorption Hysteresis in Amorphous, Microporous Polymeric Materials. *Langmuir* **2013**, *29*, 12982–12989. [CrossRef] [PubMed]

38. Adhikary, J.; Meistelman, M.; Burg, A.; Shamir, D.; Meyerstein, D.; Albo, Y. The Reductive De-halogenations of Mono and Tribromo Acetic Acids by $NaBH_4$ Catalysed by Gold Nanoparticles Entrapped in Sol-Gel Matrices Follow Different Pathways. *Eur. J. Inorg. Chem.* **2017**, *2017*, 1510–1515. [CrossRef]

39. Trabelsi, K.; Meistelman, M.; Ciriminna, R.; Albo, Y.; Pagliaro, M. Effective and Green Removal of Trichloroacetic Acid from Disinfected Water. *Materials* **2020**, *13*, 827. [CrossRef]

40. Song, J.; Huang, Z.F.; Pan, L.; Li, K.; Zhang, X.; Wang, L.; Zou, J.J. Review on selective hydrogenation of nitroarene by catalytic, photocatalytic and electrocatalytic reactions. *Appl. Cat. B* **2018**, *227*, 386–408. [CrossRef]

41. Qin, C.; Zhang, J.; Zhang, C.; He, Y.; Tratnyek, P.G. Abiotic Transformation of Nitrobenzene by Zero Valent Iron under Aerobic Conditions: Relative Contributions of Reduction and Oxidation in the Presence of Ethylene Diamine Tetraacetic Acid. *Environ. Sci. Technol.* **2021**, *55*, 6828–6837. [CrossRef]

42. Machado, S.A.S.; Avaca, L.A. The hydrogen evolution reaction on nickel surfaces stabilized by H-absorption. *Electrochim. Acta* **1994**, *39*, 1385–1391. [CrossRef]

43. He, F.; Gong, L.; Fan, D.; Tratnyek, P.G.; Lowry, G.V. Quantifying the efficiency and selectivity of organohalide dechlorination by zerovalent iron. *Environ. Sci. Process. Impacts* **2020**, *22*, 528–542. [CrossRef] [PubMed]

44. Agrawal, A.; Tratnyek, P.G. Reduction of Nitro Aromatic Compounds by Zero-Valent Iron Metal. *Environ. Sci. Technol.* **1995**, *30*, 153–160. [CrossRef]

45. Bae, S.; Gim, S.; Kim, H.; Hanna, K. Effect of $NaBH_4$ on properties of nanoscale zero-valent iron and its catalytic activity for reduction of p-nitrophenol. *Appl. Cat. B* **2016**, *182*, 541–549. [CrossRef]

46. Andreou, D.; Iordanidou, D.; Tamiolakis, I.; Armatas, G.S.; Lykakis, I.N. Reduction of Nitroarenes into Aryl Amines and N-Aryl hydroxylamines via Activation of $NaBH_4$ and Ammonia-Borane Complexes by Ag/TiO_2 Catalyst. *Nanomaterials* **2016**, *6*, 54. [CrossRef]

47. Abdelhamid, H.N. A review on hydrogen generation from the hydrolysis of sodium borohydride. *Int. J. Hydrog. Energy* **2021**, *46*, 726–765. [CrossRef]

48. Karimadom, B.R.; Meyerstein, D.; Kornweitz, H. Calculating the adsorption energy of a charged adsorbent in a periodic metallic system—The case of $BH_4{}^-$ hydrolysis on Ag(111) surface. *Phys. Chem. Chem. Phys.* **2021**. [CrossRef]

49. Sermiagin, A.; Meyerstein, D.; Bar-Ziv, R.; Zidki, T. The Chemical Properties of Hydrogen Atoms Adsorbed on M°- Nanoparticles Suspended in Aqueous Solutions: The Case of Ag°-NPs and Au°-NPs Reduced by $BD_4{}^-$. *Angew. Chem. Int. Ed.* **2018**, *57*, 16525. [CrossRef]

50. Mondal, T.; Sermiagin, A.; Meyerstein, D.; Zidki, T.; Kornweitz, H. On the mechanism of reduction of $M(H_2O)_m{}^{n+}$ by borohydride: The case of $Ag(H_2O)_2{}^+$. *Nanoscale* **2020**, *12*, 1657–1672. [CrossRef]

51. Rolly, G.S.; Meyerstein, D.; Yardeni, G.; Bar-Ziv, R.; Zidki, T. New insights into HER catalysis: The effect of nano-silica support on catalysis by silver nanoparticles. *Phys. Chem. Chem. Phys.* **2020**, *22*, 6401–6405. [CrossRef] [PubMed]

52. Gu, C.; Jia, H.; Li, H.; Teppen, B.J.; Boyd, S.A. Synthesis of highly reactive subnano-sized Zero-Valent Iron using smectite clay templates. *Environ. Sci. Technol.* **2010**, *44*, 4258–4263. [CrossRef]